RSC Advances

PAPER

View Article Online
View Journal | View Issue

Open Access Article. Published on 17 February 2025. Downloaded on 1/22/2026 7:04:25 AM.
This article is licensed under a Creative Commons Attribution-NonCommercial 3.0 Unported Licence.

Check for updates

Cite this: *RSC Adv.*, 2025, **15**, 5264

Wettability modification of a nano-silica/fluoro surfactant composite system for reducing the damage of water blocking in tight sandstone reservoirs

Cen Chen,[a] Seqiang Zhuo,[b] Songze Li,*[a] Nanxin Yin,[a] Chao Luo,[a] Hong Ren,[c] Min Jia,[d] Xinyue Wang[a] and Qun Cheng[e]

In the process of drilling and development of tight sandstone reservoirs, a large number of external fluids can invade the pore structure of the reservoir due to its strong hydrophilicity, resulting in blockage of the pore structure and a decrease in oil and gas production capacity. To reduce the aqueous phase trapping damage of tight sandstone reservoirs, the SiO_2@KH550/FC-A nano-composite system was prepared to construct hydrophobic surfaces in core samples. First, the surface of nano-SiO_2 was modified by KH550 to prepare nanoparticles with good dispersion. FTIR, XRD, SEM, and TG were used to characterize the nanoparticles before and after modification. The fluorosurfactant FC-A was prepared in the laboratory and combined with SiO_2@KH550 to produce the SiO_2@KH550/FC-A composite system. The system increases the contact angle of the hydrophilic surface from approximately 20° to 130°, achieving wetting modification. Excellent stability of hydrophobicity was obtained, and the contact angle did not significantly decrease within 5 minutes. In contrast, using FC-A and SiO_2@KH550 individually, the contact angle of the hydrophilic surface could not be increased to over 90°. The SEM results showed that after treatment with the composite system, a layer of micro–nanoscale particles was attached to the hydrophilic surface. It was proved that SiO_2@KH550 and FC-A were adsorbed on the surface, forming a low surface free energy solid interface at the micro and nano scales, which greatly improved the surface hydrophobicity. Furthermore, after the composite system was used to treat tight sandstone cores aged at 100° for 16 hours, the amount of imbibition of the core samples treated with SiO_2@KH550/FC-A significantly decreased from 2.6 mL of brine to only 0.5 mL after 8 hours. The core spontaneous imbibition rate was also reduced to 0.0004 g min^{-1} within 5 minutes, while the maximum brine water spontaneous imbibition rate was 0.27 g min^{-1}. The core displacement experiment further showed that the fluid in the core pores can be more easily flowed back under gas displacement after wetting modification. The water saturation of the core samples decreased to 16.3% after displacement, and the core permeability recovered to 88.4%, indicating that the SiO_2@KH550/FC-A composite system can significantly improve the liquid phase flowback ability.

Received 4th December 2024
Accepted 27th January 2025

DOI: 10.1039/d4ra08564g

rsc.li/rsc-advances

1 Introduction

With the increasing demand for energy, the development of conventional reservoir oil and gas has gradually failed to produce sufficient energy to meet the needs of worldwide consumption. A tight sandstone reservoir is an unconventional reservoir with abundant oil and gas reserves.[1,2] However, in the process of drilling and development of tight sandstone reservoirs, a large number of external fluids invade the pore structure of the reservoir due to its strong hydrophilicity, resulting in an increase in water saturation. Moreover, due to high capillary forces, it is difficult for intrusive fluids to be removed from the reservoir, depending on formation pressure during the oil/gas development.[3,4] As a result, the invading fluid is trapped in the reservoir, causing blockage of the pore structure, which results in a decrease in oil and gas production capacity.[5] Liquid phase trap damage is very severe for oil and gas production during the development of tight sandstone reservoirs.[4–6]

At present, the method of adding surfactants to fluids is widely used.[7–12] Surfactants can reduce the surface tension of fluids and improve the flowback efficiency, thereby reducing

[a]Chongqing University of Science and Technology, China. E-mail: songze83@cqust.edu.cn
[b]Guangxi Shale Gas Exploration and Development Co., Ltd, China
[c]Exploration and Development Research Institute, Zhongyuan Oilfield Company, China
[d]Petroleum Engineering Technology Research Institute of Jiangsu Oilfield, China
[e]JinFeng Laboratory, China

© 2025 The Author(s). Published by the Royal Society of Chemistry

Open Access Article. Published on 17 February 2025. Downloaded on 1/22/2026 7:04:25 AM.
This article is licensed under a Creative Commons Attribution-NonCommercial 3.0 Unported Licence.

possible liquid phase trapping damage. However, the effect of surfactants is insufficient. In addition, surfactants are prone to foaming, resulting in the formation of a Jamin effect in the formation pores, which further reduces the permeability.[8,9,11]

Wetting inversion technology has been gradually proposed and applied in oil and gas exploitation.[13–15] At present, wetting inversion is mainly achieved by chemical agents such as surfactants, nanofluids, and polymers. Cationic surfactants, cationic and non-ionic surfactant combined systems, and fluorinated surfactants can modify water-wet surfaces to neutral wetting surfaces.[7–10,12–15] In addition to traditional surfactants, researchers continue to develop new surfactants for increased wettability and adaptability. For example, there is considerable temperature resistance and salt resistance exhibited by zwitterionic surfactants and Gemini surfactants,[16,17] and they can play a role in complex reservoir environments.

Nanoparticles can form an adsorption layer on a rock surface and change the physical and chemical properties of the surface, so as to achieve altered wettability. For example, some metal oxide nanoparticles, such as silica and alumina, can adsorb on the reservoir rock surface and change its wettability.[11,18,19] A common procedure researchers have used is the optimization of the material composition and properties of nanofluids. The wetting inversion effect and stability of nanofluids can be improved by adjusting the type, size, concentration, and other parameters of nanoparticles, as well as compounding with other chemical agents. New nanomaterials and nanofluid systems have also been developed to meet the application requirements under different reservoir conditions.[20–24]

A synergistic effect is obtained when a surfactant is mixed with other chemical agents or nanomaterials to improve the wetting alteration effect. For example, fluids mixed with surfactants and nanomaterials employ the wettability of surfactants, and also exhibit the structural and interface characteristics of nanomaterials, so as to better realize the wettability alteration of the reservoir. In this study, nano-silica powder was modified to improve the dispersion of nanoparticles, and after it was mixed with fluorine-containing anionic surfactants, the wetting alteration ability of the composite system was then studied. Furthermore, by means of advanced microscopic characterization techniques, including scanning electron microscopy (SEM), the adsorption behavior and wettability change process of the wetting alteration agent on the rock surface were revealed, which provided strong support for the study of wetting inversion technology.

2 Materials and methods

2.1 Materials

Nano-SiO_2 was purchased from the Xianfeng Nanometer Materials Co., Ltd, Nanjing, China. KH550 and absolute ethanol were purchased from Shanghai Aladdin Biochemical Technology Co., Ltd (Shanghai, China). FC-A is an analytic reagent, and the production factory is the Beijing FLUOBON Surfactant Institute. The chemical structure of FC-A is shown in Fig. 1. The surfactant concentration was obtained using the mother's liquid dilution method. The deionized water was prepared in our laboratory.

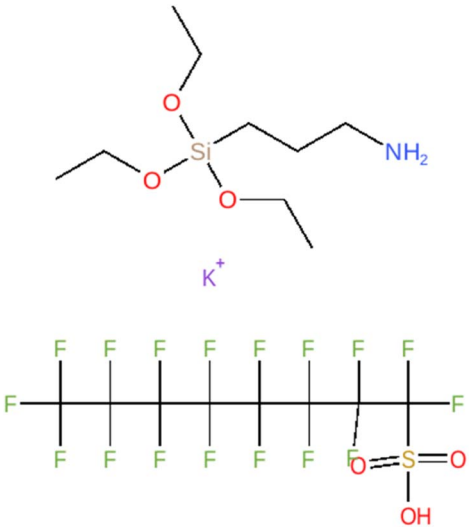

Fig. 1 The chemical structures of KH550 and FC-A.

We selected typical tight sandstone for the wettability and core flow tests. The core characteristics are shown in the table below. A mica plate was used for the wettability evaluation and SEM test. Because mica is similar to the mineral component and wettability of the actual core samples, and its surface is slippery, it is easier to study the adsorption characteristics. Mica chips with the length and width of 1.5 cm × 1.5 cm were used after fresh stripping. The physical properties of core samples are described in Table 1.

2.2 Synthesis of SiO_2@KH550 and preparation of the SiO_2@KH550/FC-A system

Because of the large number of active hydroxyl groups on the surface of nano-silica and its strong hydrophilicity, agglomerates or secondary aggregates easily form that are not conducive to its dispersion in the material, and then can affect the structure and properties of the material. Therefore, it is necessary to modify the surface of nano-silica to ensure its stable storage and improve its dispersibility in the polymer matrix. To increase the dispersibility of nano-silica and its compatibility with the organic matrix, it is necessary to modify the surface of silicon dioxide to weaken its polarity and reduce its energy state.

SiO_2@KH550 can be obtained by the surface modification method using the KH550 silane coupling agent. This method can significantly improve the dispersibility and stability of nano-silica in water-based media, and enhance its compatibility with organic polymer materials, so as to improve the performance of composite materials. KH550 is an organosilicon compound. By reacting the KH550 silane coupling agent with the hydroxyl group on the surface of nano-silica, the surface of nano-silica can be converted to alkoxy silane, thus achieving surface modification.

SiO_2 is activated by drying at 40 °C for 48 h, which ensures the activation of necessary functional groups. The dried SiO_2

Open Access Article. Published on 17 February 2025. Downloaded on 1/22/2026 7:04:25 AM.
This article is licensed under a Creative Commons Attribution-NonCommercial 3.0 Unported Licence.

Table 1 The physical properties of the core samples and relative imbibition fluid used

Core sample	Porosity [φ]/%	Permeability [k]/md	Length [L]/cm	Diameter [D]/cm	Imbibition fluid used
1-1#	6.64	0.0236	5.148	2.494	SI in brine water
1-2#	7.28	0.0523	5.192	2.506	SI in FC-A
2-1#	6.62	0.0285	4.496	2.502	SI in SiO_2@KH550
2-2#	6.71	0.0332	5.190	2.504	SI in SiO_2@KH550/FC-A
3-1#	5.88	0.0765	5.044	2.502	CD in brine water
3-2#	6.72	0.0662	5.124	2.506	CD in FC-A
4-1#	7.13	0.0512	5.142	2.496	CD in SiO_2@KH550
4-2#	5.97	0.0327	5.060	2.508	CD in SiO_2@KH550/FC-A

was then mixed with deionized water and anhydrous ethanol in a flask, and a satisfactory dispersion was reached by ultrasonic stirring for 2 hours (as shown in Fig. 1). Then, KH550 (3 wt%) was added, and the solution was stirred for 30 minutes. After the system was evenly mixed, the reactor was heated in a water bath kettle at 80–90 °C for 4 hours to promote the required chemical interaction between SiO_2 and KH550. Finally, the nano-powder was washed with anhydrous ethanol three times, and then the product was dried at 100 °C for 3 hours to obtain the sample, which was recorded as SiO_2@KH550.

After SiO_2@KH550 was thoroughly stirred and ultrasonically dispersed, lab-synthesized FC-A was added to the suspension to form the SiO_2@KH550/FC-A composite system. A schematic diagram of the entire process for preparing SiO_2@KH550/FC-A is shown in Fig. 2.

2.3 Structural characterization of SiO_2@KH550/FC-A

2.3.1 Fourier transform infrared (FT-IR) spectroscopy. Fourier transform infrared spectroscopy was utilized to determine the molecular structure of the prepared SiO_2@KH550. The FT-IR spectra were obtained by the KBr press method with a scanning range of 400–4000 cm^{-1} and a resolution of 4 cm^{-1}.

2.3.2 XRD. Changes in the crystal structure of SiO_2 and SiO_2@KH550 were analyzed by polycrystalline X-ray diffraction (XRD). Herein, XRD analysis was conducted using a Bruker D8-Advance XRD diffractometer (Dresden, Germany).

2.3.3 Particle size. The particle size distribution of the nanoparticles before and after modification was tested using a Bruker particle size tester. The concentration of the nanofluid was 0.05%, and the test medium was water.

2.3.4 SEM. The morphology of nanoparticles before and after modification was determined by field emission scanning electron microscopy (FE-SEM, Hitachi UHR SU8010, Japan).

2.4 Method of wettability alteration

2.4.1 Contact angles. The static contact angle of the water–gas–rock system was measured by contact angle tester to evaluate the effect of wetting modification. The contact angle of the interface between the surfactant solution–gas–solid system was measured by a contact angle measurement setup (JC2000D5M, China). The rock samples were cut into square slices with the thickness of 0.5 cm and length of 2 cm. In addition, to minimize the impact of rock roughness on wettability, the oxide film was removed, and then, the rock was gradually polished with 2000 grit sandpaper, rinsed with 3% boiled NaOH solution, and dried in an oven at 105 °C.

After that, the initial contact angles of the core samples were tested. Each sample was measured three times, and the average value was taken. A suspension of 1% nano SiO_2@KH550, 0.1%

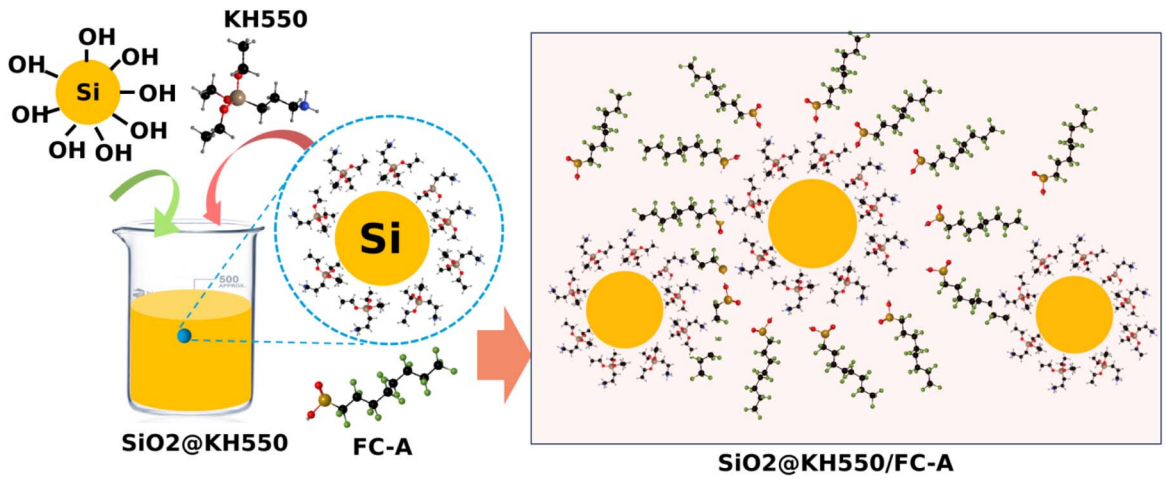

Fig. 2 Schematic diagram of the reaction process of modification of SiO_2@KH550 and the SiO_2@KH550/FC-A system.

 © 2025 The Author(s). Published by the Royal Society of Chemistry

Open Access Article. Published on 17 February 2025. Downloaded on 1/22/2026 7:04:25 AM.
This article is licensed under a Creative Commons Attribution-NonCommercial 3.0 Unported Licence.

FC-A solution, and 1% SiO_2@KH550 + 0.1% FC-A composite system was prepared. Then, three fresh mica sheets were placed on the systems for adsorption for 24 hours. After the mica sheets treated with the various systems were dried, they were employed to measure the contact angles using deionized water droplets, and contact angle images were recorded.

2.4.2 Spontaneous imbibition tests. The change in the core imbibition rate with time before and after the wettability alteration was recorded by the spontaneous imbibition dynamic process. The detailed method is as follows:

(1) The rock sample to be tested was dried so that the initial saturation of all samples remained at a consistent level. The drying temperature of the rock sample was not higher than 80 °C (with fluctuation less than ±5 °C), and the core mass was weighed at intervals until the difference between the two weighings was less than 10 mg.

(2) The length, diameter, and weight of the dried rock sample were measured.

(3) The core was hung on a clamp at the top end of the balance, and the end face was maintained parallel to the liquid surface in the container. Then, the platform was slowly raised until it contacted the end face of the core sample. At this time, the spontaneous imbibition dynamic process began, and the data generated by the balance was recorded over time. During the course of imbibition, the side surfaces of the core plugs were sealed with epoxy to minimize the experimental error caused by evaporation.

2.5 Core displacement test

After measuring pore permeability parameters and other characteristics, the core samples were dried under vacuum, and then saturated with brine water to simulate oil field water. Brine water was used to maintain the equivalent salinity of the formation, thus avoiding the degradation of the pore structure of the core due to salinity sensitivity.

Displacement tests were carried out under different pressure differences. Under each pressure difference, gas flooding tests were conducted to reach the unchanged flooding volume. Fig. 3 shows a diagram of the gas displacement device. First, the core samples were dried in a vacuum, and the size and quality were measured. The core samples were then soaked in various systems and aged at 120 °C for 24 hours to achieve adsorption equilibrium. The treated core samples were taken out to dry and saturated with brine. The core was placed in a core holder, and was driven forward to stability under different pressure differences.

Gas permeabilities were measured before and after the test, and weighed and recorded after the displacement. When the inlet pressure changed, it was ensured that the confining pressure was 1.5 times that of the inlet pressure to prevent the gas from leaking out from the side and causing errors in the permeability test. The quality of the fluid loss flowing out of the outlet and permeability were tested and recorded.

The brine water was collected from the formation in an oil reservoir in China. The detailed ionic composition of the water appears in Table 2.

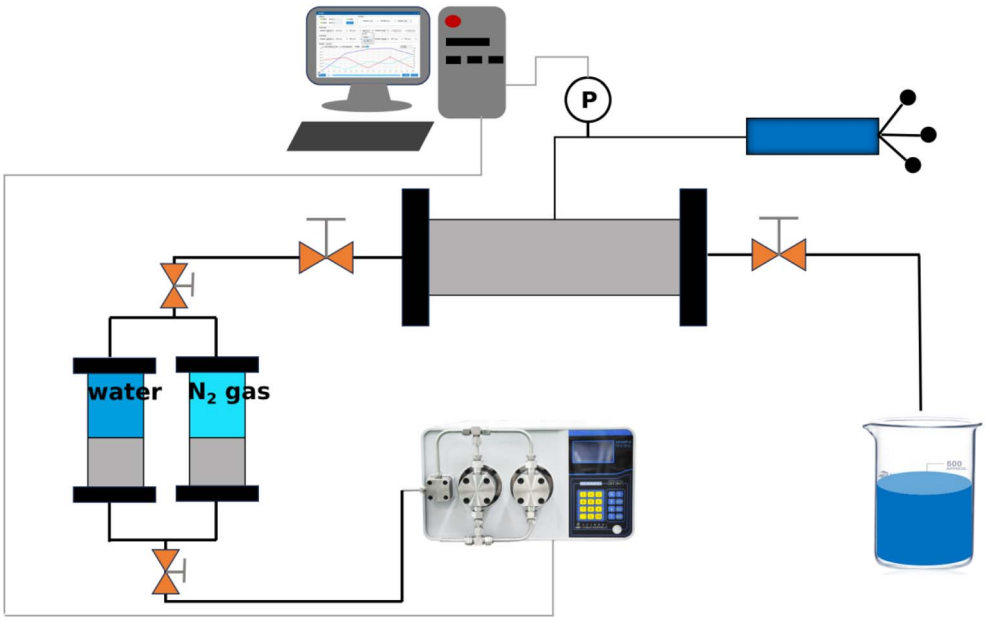

Fig. 3 A diagram of the gas displacement device.

Table 2 The ionic composition of brine water

Cl^- (mg L^{-1})	CO_3^{2-} (mg L^{-1})	HCO_3^- (mg L^{-1})	SO_4^{2-} (mg L^{-1})	Br^-	Ca^{2+}	Mg^{2+}
9839.09	45.34	125.39	1843.56	10.43	642.94	459.41

Open Access Article. Published on 17 February 2025. Downloaded on 1/22/2026 7:04:25 AM.
This article is licensed under a Creative Commons Attribution-NonCommercial 3.0 Unported Licence.

Brine water was used to maintain the same salinity as the formation, thus preventing degradation of the pore structure of the core due to salinity sensitivity. This ensures that the core samples will not be affected by sensitivity during imbibition and core displacement tests.

3 Results

3.1 Characterization of SiO_2@KH550

3.1.1 FT-IR. The structural spectrum of the nanomaterials was determined by FT-IR. Fig. 4 shows the infrared spectrum of SiO_2 with a strong wide peak at 3483 cm^{-1}, which is the –OH stretching vibration peak. Compared with SiO_2@KH550, the peak strength was weakened, indicating that the strength of the hydrophilicity of nano-SiO_2 was weakened, and the –Si–OH structural units were reduced during the modification process. After SiO_2 was modified, an acromion appeared at 973 cm^{-1}, indicating that KH550 successfully modified the nano-SiO_2. An Si–O–Si antisymmetric vibration peak appeared at 1140 cm^{-1}. Additionally, 960 cm^{-1} is the absorption peak of the Si–OH bending vibration, and 798 cm^{-1} is the peak of the Si–O–Si symmetric tensile vibration.

3.1.2 XRD. Changes in the crystal structure of SiO_2 and SiO_2–KH550 were analyzed by XRD. The XRD patterns of SiO_2 and SiO_2@KH550 in Fig. 5 show that the corresponding patterns of all samples included a wide peak in the diffraction angle range of 15–28, which denotes the standard amorphous peaks of SiO_2. This indicates the amorphous structures of SiO_2 and SiO_2@KH550. SiO_2 and SiO_2@KH550 are in the amorphous state and are in the form of nano-scale spherical particles. The stability of amorphous SiO_2 is excellent, with uniform dispersion and a large number of active sites, which is conducive to uniform distribution on a solid surface. These results show that the structural integrity of the SiO_2 particles was not affected, despite the modification by the KH550.[25,26]

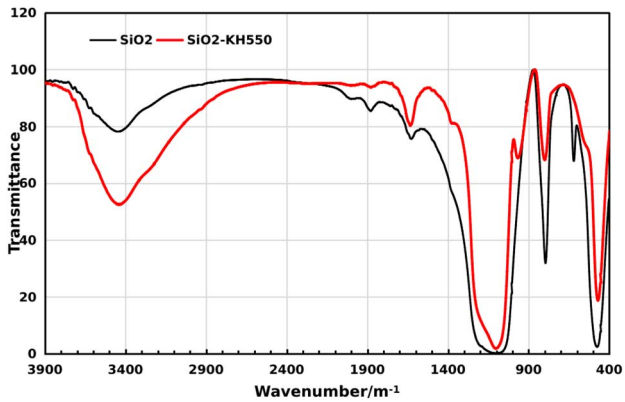

Fig. 4 Fourier-transform infrared (FT-IR) spectra of SiO_2 and SiO_2@KH550.

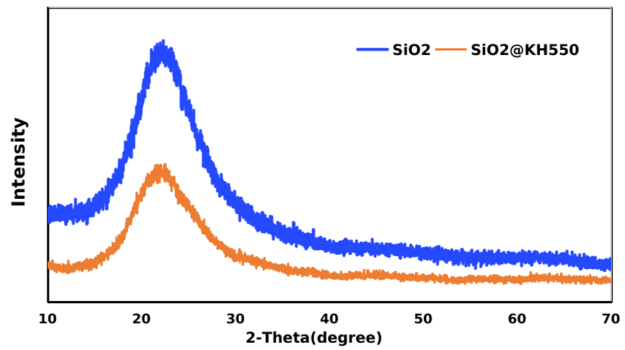

Fig. 5 The XRD patterns of SiO_2 and SiO_2@KH550.

3.1.3 Distribution of particle size and zeta potential. The particle sizes of nano-silica and modified SiO_2@KH550 were tested and analyzed, as shown in Fig. 6(a). The results showed that there was less dispersion of nano-silica in water, and the particle size distribution was uneven with a wide dispersion coefficient, indicating that the surface energy of unmodified nano-silica is high and the hydrophilicity is strong, thus resulting in easier agglomeration of nanoparticles and large particle size. However, the dispersion of nano-silica modified by KH550 in water significantly increased. The particle size distribution showed that the average particle size was 40 nm and the dispersion coefficient was 0.02, which indicates that the surface energy of nano-silica particles decreased, and the agglomeration between particles also decreased, resulting in the advanced dispersion. The excellent dispersion can provide a basis for the construction of micro–nano rough surfaces.

3.1.4 SEM. The surface morphology of nano-silica before and after modification was determined by SEM. Fig. 6(b) shows a high-definition morphology image of SiO_2@KH550 with excellent dispersion. As shown in Fig. 6(c) and (d), the untreated nano-silica particles often gathered together to form large clusters due to the high surface energy of the nanopowder, which is good for the minimum energy due to the attraction by the van der Waals forces. This leads to decreased dispersion of the nanoparticles, which cannot form a uniform micro/nanoscale structure on the solid surface. While the nano-silica was modified by KH550, as shown in the figure, large clusters are not in the field of view, suggesting that the dispersion of nanoparticles was significantly increased.[17,18] This occurred mainly because the nanoparticles are dispersed in water due to the steric hindrance and electrostatic repulsion of KH550 on the SiO_2 surface. The results showed that the surface of nano-SiO_2 was successfully modified, and the dispersibility was enhanced.

3.2 Contact angle

3.2.1 The effect of concentration on contact angle. The surface of hydrophilic mica was treated with different concentrations of modified nano-silica, fluorinated anion surfactant, and composite system, and the change in the contact angle before and after treatment was compared to analyze the wettability of the composite system on the surface of hydrophilic mica.

First, the effect of the concentration of FC-A on the contact angle was studied. Fig. 7 shows that with increasing concentration, the contact angle of the solid surface after FC-A treatment initially increases and then decreases, and the maximum

 © 2025 The Author(s). Published by the Royal Society of Chemistry

Open Access Article. Published on 17 February 2025. Downloaded on 1/22/2026 7:04:25 AM.
This article is licensed under a Creative Commons Attribution-NonCommercial 3.0 Unported Licence.

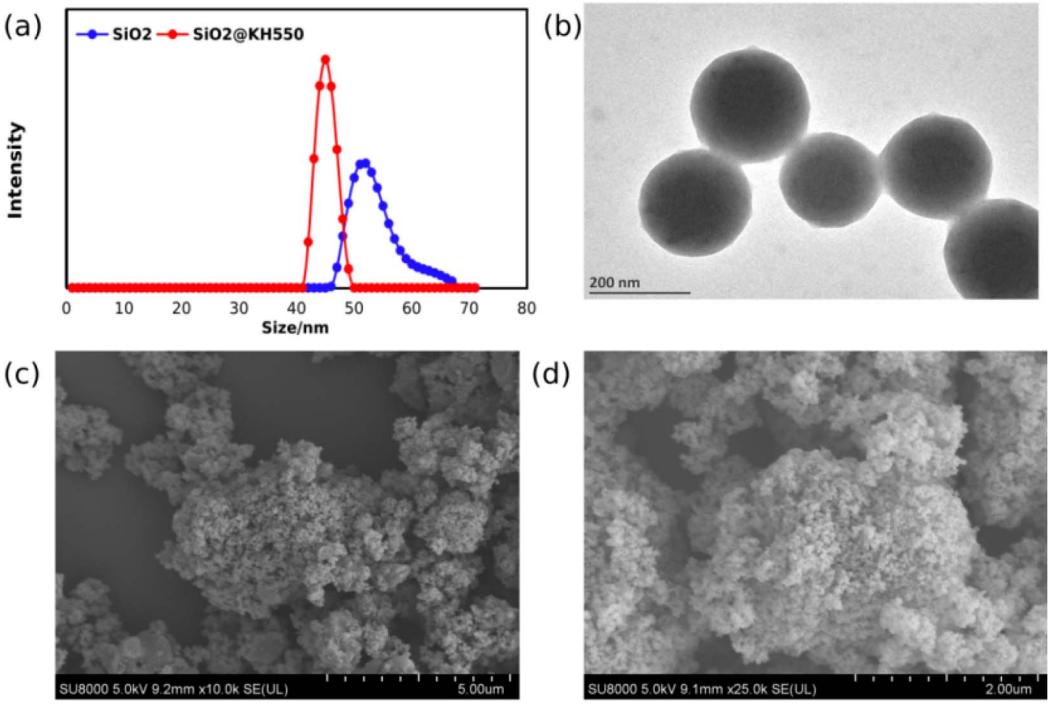

Fig. 6 (a) The particle size distribution for SiO_2 and SiO_2@KH550. (b) The surface morphology of dispersed SiO_2@KH550. (c) The surface morphology of SiO_2. (d) The surface morphology of SiO_2@KH550.

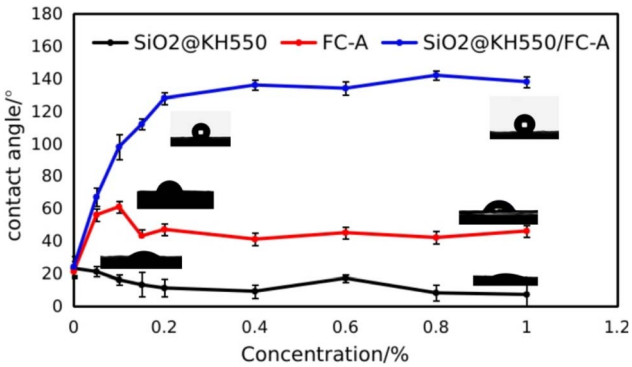

Fig. 7 The variation in contact angles with the concentration of different fluids.

value occurs when the concentration is approximately 0.1%, which is approximately 68°. The error bar indicates that the experimental error is small, and the results can be regarded as a statistical regularity. This is mainly because the adsorption of FC-A on the surface of mica as a surfactant conforms to the Langmuir isothermal adsorption model. At low concentrations, FC-A molecules are adsorbed as a monolayer, and the adsorption amount on the solid surface is relatively low, which indicates that the hydrophilic head group of FC-A molecules can be adsorbed on the solid surface, and the entire molecule lies sparsely on the solid surface due to the low distribution density. When the concentration increases, the adsorption capacity of FC-A molecules increases, resulting in the vertical establishment of FC-A molecules on the solid surface, exposing the hydrophobic chain on the solid surface and increasing the surface hydrophobicity. However, because FC-A is an anionic surfactant, the adsorption capacity of FC-A is relatively lower due to the electrostatic repulsion on the surface of the molecules and the solid matrix.

The effect of SiO_2@KH550 concentration on the contact angle was studied, and the results are shown in Fig. 7. When the concentration of SiO_2@KH550 increases, the contact angle clearly decreases, and all of samples are strongly hydrophilic (less than 20°). This is mainly due to the construction of micro–nano structures on the solid surface by nanoparticles, resulting in an increase in the contact area of the solid and liquid. Moreover, with the increase in the concentration, the nanoparticles deposited and accumulated, resulting in more obvious surface roughness and decreased contact angles. This also reveals that micro–nano rough structures can be formed that support the subsequent construction of low-surface energy solid surfaces based on the micro–nano rough structures.

Furthermore, the effect of composite system concentration on the contact angle was studied. The results are shown in Fig. 7 with a fixed concentration of 0.05% for SiO_2@KH550. The contact angle of the mica sheet treated by the composite system without FC-A remained at 22°, and with increasing concentration of FC-A, the contact angle of the mica treated by the composite system rapidly increases. When the concentration of FC-A reaches 0.2%, the contact angle increases to 128°. As the concentration continues to increase, the contact angle of the system gradually becomes stable. The results showed that the SiO_2@KH550/FC-A composite system can significantly increase the contact angle and modify the wettability from hydrophilicity to hydrophobicity.[11,12,19]

Open Access Article. Published on 17 February 2025. Downloaded on 1/22/2026 7:04:25 AM.
This article is licensed under a Creative Commons Attribution-NonCommercial 3.0 Unported Licence.

3.2.2 The stability of water contact angles. Furthermore, the stability of water contact angles of mica treated by various systems was analysed, as shown in Fig. 8. According to the results, when water was dropped onto the surface of an untreated fresh mica sheet, the water drops rapidly spread on the surface, and after 10 s of stability, the contact angle was only 21°, showing strong hydrophilicity. The results show that the contact angle of the SiO_2@KH550-treated mica sheet surface rapidly decreased from 19° to 7° within 30 s, which was smaller than that of the untreated mica sheet surface. This indicates that the surface hydrophilicity of the mica sheet increased further after being treated with SiO_2@KH550. Thus, SiO_2@KH550 is adsorbed onto the surface of the mica sheet, which increases the hydrophilic groups on the surface of the mica sheet. The nanoparticles increase the surface roughness, which causes water droplets to spread faster. When fresh mica was treated with 0.1% FC-A, the contact angle increased to 53°, and then remained nearly unchanged within 90 s. This occurred because the FC-A hydrophilic group was adsorbed onto the surface of the mica sheet, and the hydrophobic chain containing fluorine faces outward, resulting in weakened hydrophilicity.

According to studies, the adsorption of surfactants is the reason for the change in wettability. However, because FC-A is an anionic surfactant, there is electrostatic repulsion between the anionic group of its head group and the negatively charged sandstone surface, resulting in low adsorption of FC-A. Therefore, the surface of the substrate treated with FC-A continued to show hydrophilicity. Finally, after the mica was infiltrated by the SiO_2@KH550/FC-A composite system for 24 h, the contact angle of the mica surface significantly increased, reaching up to 132°, and showing a hydrophobic surface. The wettability of mica treated by the SiO_2@KH550/FC-A composite system showed excellent durability with no changes after 5 min.

According to the results of the contact angle change over time, the contact angle did not change with time, and the hydrophobic surface was stable. The results showed that the hydrophilic surface can be modified to a hydrophobic surface by the composite system.

3.2.3 Micro-mechanism of wettability alteration. It is well known that the surface micro–nanostructures of hydrophobic materials[12,17,19] play a crucial role in their wettability. Therefore, the morphology and microstructure of SiO_2 and SiO_2@KH550/FC-A were preliminarily studied. Typical SEM images showed that when the concentration was high, the surface morphology was uneven, with severe clumping, which was mainly formed by the aggregation of small spherical nanoparticles, as shown in Fig. 9(a). The surface morphology showed that uniform micro–nanostructures formed with difficulty on the surface, and therefore, the wettability did not increase.

After modifying SiO_2, organic groups were grafted onto the surface of SiO_2, which enhanced its dispersion and hydrophobicity, and altered the morphology of the surface composition with increased uniformity and the formation of micro and nanostructures. The gap between these micro and nanoparticles trapped air to form an air cushion where water droplets were suspended at the gas–solid–liquid interface, while the FC-A surfactant reduced the surface free energy. The mapping results in Fig. 9(e) show that Si, F, Al, and O are the main elements of the nanomaterial loaded on the matrix surface, which proves that the fluorine surfactant and nanomaterial were simultaneously adsorbed on the matrix surface.

3.3 Capillary force

Capillary force is the pressure difference between the non-wet phase and the wet phase on both sides of the curved surface in a capillary tube, and the additional pressure produced by the joint action of wetting tension and interfacial tension on the curved surface. The values of the capillary force are proportional to the cos θ and surface tension (σ), and inversely proportional to the radius (r). The calculation formula for capillary force is as follows:

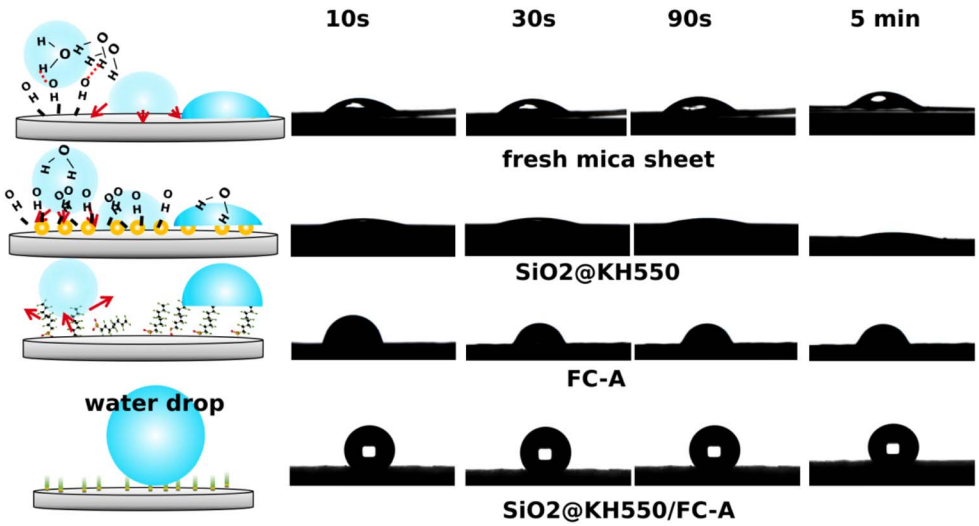

Fig. 8 The stability of water contact angles of mica treated with various fluids.

 © 2025 The Author(s). Published by the Royal Society of Chemistry

Open Access Article. Published on 17 February 2025. Downloaded on 1/22/2026 7:04:25 AM.
This article is licensed under a Creative Commons Attribution-NonCommercial 3.0 Unported Licence.

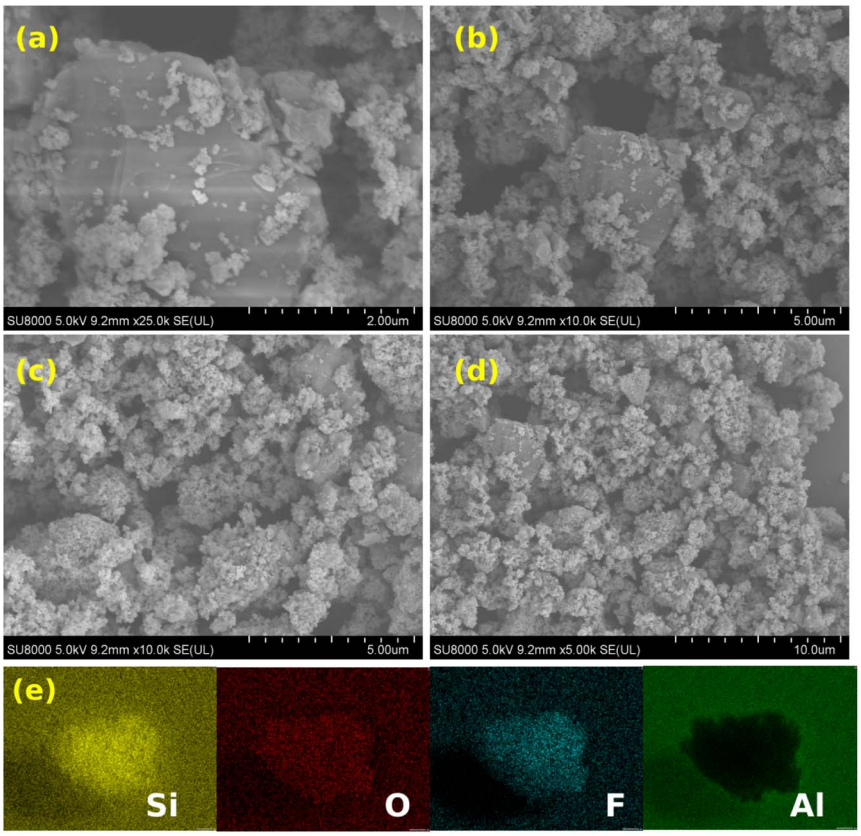

Fig. 9 The surface morphology of a hydrophilic solid treated with (a) SiO_2, (b) SiO_2@KH550, and (c and d) SiO_2@KH550/FC-A. (e) SEM mapping images.

$$P_c = \frac{2\sigma \cos\theta}{r} \quad (1)$$

where P_c denotes the capillary force, σ denotes the interfacial tension, denotes the contact angle, and r denotes the capillary radius.

Fig. 10 shows that surface tensions are related to surfactant concentrations at different concentrations of FC-A and the SiO_2@KH550/FC-A composite system. The results showed that surface tensions gradually decreased with increasing concentration. Until the concentration reached the critical micelle concentration (CMC), the surface tension remain stable. The surface tension of FC-A is lower than that of the SiO_2@KH550/FC-A system because the FC-A is adsorbed on the nanoparticle surface, reducing its effective concentration in solution.

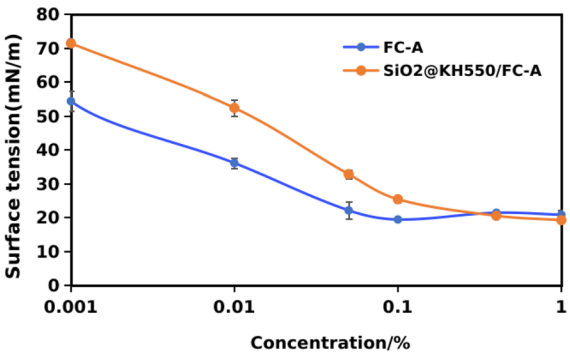

Fig. 10 Surface tensions with different concentrations of FC-A and the SiO_2@KH550/FC-A composite system.

According to the capillary force equation, it is assumed that for the same reservoir, the capillary pore diameter can be regarded as the same, and therefore, $\sigma \cos\theta$ jointly determines the capillary force. According to the surface tension and contact angle measurements, the $\sigma \cos\theta$ of FC-A and the SiO_2@KH550/FC-A composite system at different concentrations was obtained, so as to determine the effect of the treatment agent on the capillary force. Fig. 11 shows that the $\sigma \cos\theta$ of water is approximately 65 without a treatment agent. However, the capillary force significantly decreases with increasing concentrations of FC-A or the SiO_2@KH550/FC-A composite system. When the concentration is greater than 0.1%, the $\sigma \cos\theta$ value of the SiO_2@KH550/FC-A composite system was even less than 0, which denotes the change in the capillary force in the reservoir from the driving force to the resistance force after treatment of the system. The external fluid did not enter the pore space due to the capillary spontaneous imbibition.

3.4 Spontaneous imbibition

The spontaneous imbibition test of the core can evaluate the amount of test liquid drawn in by capillary force.[3,4,20] If the amount of suction is less, the fluid occupies less of the core pore

Open Access Article. Published on 17 February 2025. Downloaded on 1/22/2026 7:04:25 AM.
This article is licensed under a Creative Commons Attribution-NonCommercial 3.0 Unported Licence.

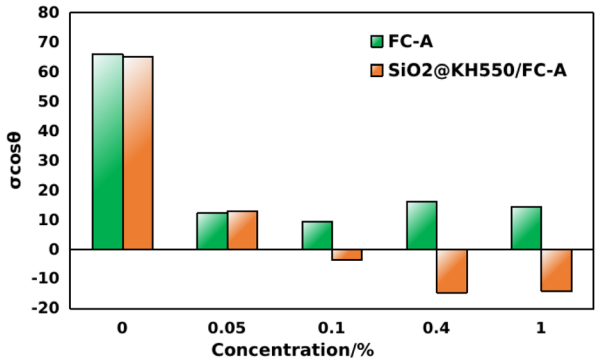

Fig. 11 Variation of $\sigma \cos \theta$ with different concentrations of FC-A and the SiO_2@KH550/FC-A composite system.

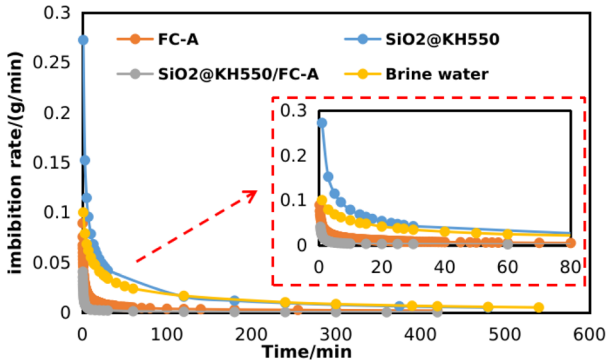

Fig. 13 Spontaneous imbibition rates of core samples treated with various fluids.

volume, and the degree of damage to the reservoir core is lower. The imbibition results for FC-A, SiO_2@KH550, and the SiO_2@KH550/FC-A composite system were evaluated and compared with simulated formation water.

Fig. 12 shows the change in the amount of spontaneous imbibition liquid with time in the process of core self-imbibition for 4 types of test fluids. The core self-imbibition process is divided into two stages, namely, the rapid self-imbibition stage that initially occurs, and the slow self-imbibition stable stage that follows. Self-imbibition water saturation with simulated formation water is the highest at any imbibition time, indicating that the core pore surface is strongly hydrophilic, and water molecules easily enter the core pore through capillary force self-imbibition.

The self-imbibition of FC-A decreased, because FC-A not only reduced the surface tension of the system, but also increased the core wettability, resulting in a decrease in capillary force. For the SiO_2@KH550 suspension, although SiO_2@KH550 will further increase the core hydrophilicity, the particle size of SiO_2@KH550 may cause a certain blockage at the throat of the core surface, resulting in a degree of imbibition that is slightly lower than that of the simulated saline imbibition. The reddish brown curve is the self-imbibition curve of the core in the SiO_2@KH550/FC-A composite system. According to the results, the self-imbibition amount for the core in the composite system is very small, only 0.5 mL after 8 hours of self-imbibition. In addition, during the self-priming process, the self-priming amount quickly becomes stable. The self-priming rate is relatively high in the first hour, and then, the curve becomes flat.

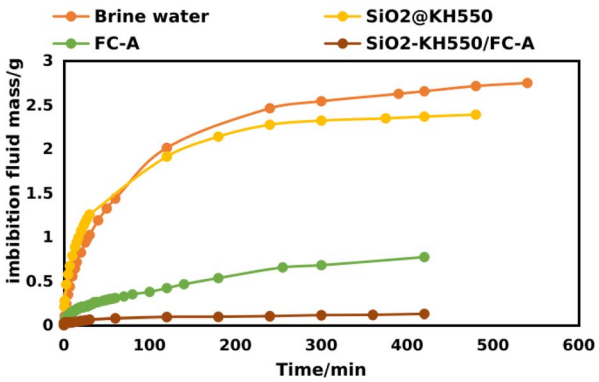

Fig. 12 The curves of spontaneous imbibition of brine water, FC-A, SiO_2@KH550, and the SiO_2@KH550/FC-A composite system.

Based on the spontaneous imbibition data, the spontaneous imbibition rates of the core samples in different liquids were calculated, and are shown in Fig. 13. The spontaneous imbibition rates of the core in brine and SiO_2@KH550 are very high, and they are maintained at a high level within the first 100 min. Compared with FC-A and the SiO_2@KH550/FC-A system, the imbibition rate of the core significantly decreases. In FC-A solution, the maximum imbibition rate is only 0.09 g min^{-1}, and rapidly decreases to 0.01 g min^{-1} within 10 min, and then is maintained at a low value. In the SiO_2@KH550/FC-A system, the maximum imbibition rate is only 0.04 g min^{-1}, and also rapidly decreases to 0.0004 g min^{-1} within 5 minutes.

These results showed that the SiO_2@KH550/FC-A system significantly reduces the core imbibition rate. The SiO_2@KH550/FC-A system subsequently forms a stable hydrophobic layer on the pore surface of the core, which significantly inhibits water entry into the pore. It is worth noting that the spontaneous imbibition rate of FC-A solution also drastically decreased. According to the capillary force equation, the capillary force is determined by surface tension and wettability. As a highly effective surfactant, FC-A can significantly reduce the surface tension and thus greatly reduce the capillary force, although it has no obvious effect on the wettability. According to Fig. 10, $\sigma \cos \theta$ can be significantly decreased from 66.1 without FC-A to 9.4 with 0.1% FC-A. Therefore, the spontaneous imbibition rate and imbibition amount of FC-A solution are significantly lower than that of brine solution.

3.5 Core displacement test and gas permeability recovery

Fig. 14 shows the variation in water saturation and gas permeability of cores treated with different systems during the core displacement experiments. According to the experimental results, in the process of continuous core displacement, the core water saturation gradually decreased, and the core permeability also recovered to a certain extent. After 0.5 MPa

 © 2025 The Author(s). Published by the Royal Society of Chemistry

Open Access Article. Published on 17 February 2025. Downloaded on 1/22/2026 7:04:25 AM.
This article is licensed under a Creative Commons Attribution-NonCommercial 3.0 Unported Licence.

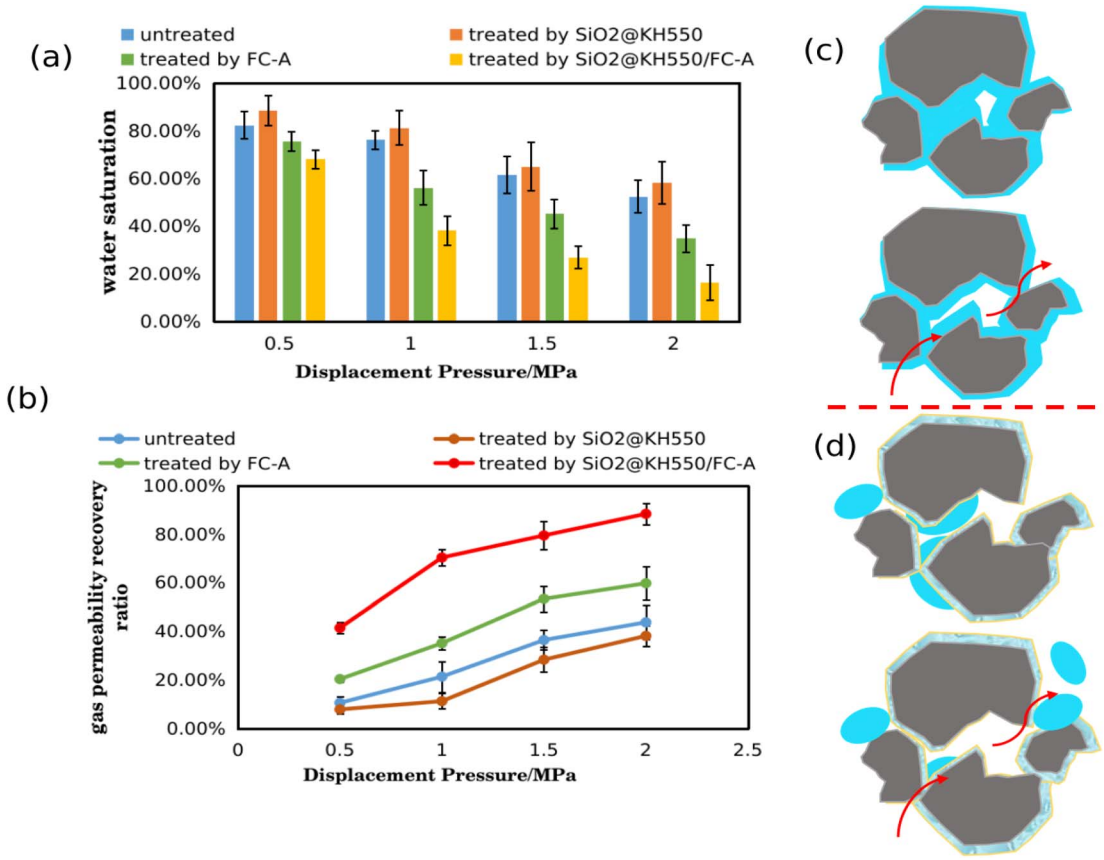

Fig. 14 The variation of (a) water saturation and (b) gas permeability of cores treated with different systems during the core displacement. Schematic illustration of the gas flooding process for an (c) untreated core sample and a (d) core sample modified by the SiO_2@KH550/FC-A system.

displacement, the water saturation of the untreated core decreased to 82.6%. After treatment with SiO_2@KH550, the water saturation of the treated core decreased to 88.7%. After FC-A treatment, the core water saturation decreased to 75.8%. However, the water saturation of the cores treated with the SiO_2@KH550/FC-A composite system significantly decreased, reaching 68.2%. When the displacement continued at 1 MPa pressure difference, the water saturation of the untreated core decreased to 72.4%. A large drop indicates that more fluid in core pores participated in the flow at 1 MPa and was driven out by gas, and the permeability also recovered accordingly.

Compared with the cores treated with SiO_2@KH550, the water saturation of the cores decreased to 77.5% at 1 MPa, indicating that stronger hydrophilicity leads to more severe liquid phase trapping. However, the water saturation of the core treated with FC-A decreased to 64.2%, and the water saturation of the core treated with the SiO_2@KH550/FC-A composite system rapidly decreased to 48.2%, with the gas phase permeability also recovering from 41.5% to 70.4%. After 1.5 MPa flooding, the water saturation of untreated and SiO_2@KH550-treated cores significantly decreased, and the permeability recovery degree increased, but the decrease in FC-A- and SiO_2@KH550/FC-A-treated cores slowed (because the absolute water saturation dropped to a relatively low value). The permeability recovery curve was still above curves 1 and 2. When the displacement pressure difference increased to 2 MPa, the water saturation of the core slowly decreased as the displacement progressed to stability, and the recovery curve for all core permeabilities entered into a stable stage. This indicated that the pores involved in the flow at the core at this stage no longer increase, the fluid that can flow no longer changes, the displacement has tended to be stable, and the remaining fluid is basically an immobile residual liquid.

Finally, after displacement, the water saturation of untreated and SiO_2@KH550-treated cores decreased to 52.6% and 58.3%, respectively, and the permeability recovered to 43.80% and 38.2%. However, the water saturation of the cores treated with FC-A and the SiO_2@KH550/FC-A composite system decreased to 34.84% and 16.3%, respectively, and the permeability recovered to 59.78% and 88.4%, indicating that the SiO_2@KH550/FC-A composite system can significantly improve the liquid phase flowback ability.

4 Discussion

The wettability of the sample was assessed by contact angle measurement. The contact angle of the hydrophilic core surface was 21°. After it was treated with SiO_2@KH550, a micro–nano

Open Access Article. Published on 17 February 2025. Downloaded on 1/22/2026 7:04:25 AM.
This article is licensed under a Creative Commons Attribution-NonCommercial 3.0 Unported Licence.

rough surface formed on its surface. However, due to the high surface energy, the contact angle remained relatively low, and the contact angle of the core was reduced to 13°. This may be due to the existence of rich hydroxyl groups on the surface of SiO_2 particles that confer hydrophilicity to SiO_2. The wettability of the hydrophobic coating was improved by adding various modifiers to change its surface properties.

The hydroxyl group on the surface of SiO_2 reacted with the organic groups on the modifier to form a three-dimensional network structure centered on Si–O–Si (composed of hydrophobic organic groups). Therefore, the core surface contact angle significantly increased after SiO_2@KH550/FC-A treatment. These results are consistent with those of surface roughness, morphology, and chemical composition. Fig. 13 shows the wetting behavior of a hydrophobic coating prepared using SiO_2@KH550/FC-A. As mentioned earlier, water tends to diffuse on smooth hydrophilic surfaces, resulting in a relatively low water contact angle in sandstone, as shown in Fig. 13. In contrast, surface roughness enhances wetting behavior. As shown in Fig. 13, the presence of SiO_2 enhanced the surface roughness, while the FC-A on the surface reduced the surface energy, resulting in an increase in the water contact angle of the coating to 110°. The protruding structure created trapped air at the interface between the droplets and the coating, impeding the diffusion of the droplets and thus increasing the contact angle. According to the Cassie–Baxter model, when the surface roughness of the material is high and the intrinsic contact angle is large, the liquid will be prevented from penetrating into the rough structure, resulting in the air being clamped and the liquid–gas contact increased. Thus, the following mathematical expression can be derived:[12,25,26]

$$\cos\theta = f_1\cos\theta_1 + f_2\cos\theta_2 \tag{2}$$

In eqn (2), θ represents the actual measured contact angle, f_1 denotes the proportion of the solid–liquid contact area, and f_2 indicates the proportion of the gas–liquid contact area, with θ_1 and θ_2 representing the contact angles between the liquid–solid and gas phases, respectively. Given that $f_1 + f_2 = 1$ and $\theta_2 = 180°$, while incorporating the roughness factor r for the solid surface, the equation can be transformed into[8] the following:

$$\cos\theta = rf_1\cos\theta_1 + f_2 \tag{3}$$

Eqn (2) and (3) show that θ_1 remains unchanged, and θ increases with decreasing f_1 value, indicating that the decrease in the solid–liquid contact area leads to an increase in the contact angle of liquid droplets on the surface of the material. Therefore, a highly hydrophobic surface with a contact angle greater than 120° can be achieved.

Fig. 15 illustrates the wettability modification induced by various fluids. After the solid surface was treated with SiO_2@KH550, rough surfaces of micro–nanostructures were constructed on the surface of the hydrophilic matrix, and the contact area between water molecules and the solid surface increased over 120°.[11] At the same time, due to the high surface energy of the nanoparticles, there was a greater attraction to water molecules.[12] Therefore, the micro–nano rough structure with a high surface energy resulted in stronger hydrophilicity. For the solid surface treated with the FC-A surfactant, the surface free energy can be significantly reduced because the hydrophobic chain of FC-A is exposed to the outside, and therefore, the hydrophilicity decreases. However, because the surface lacks a micro–nano rough structure, the wettability still cannot reach the hydrophobic FC-A.[11,18] Combined with the micro–nano rough structure of the nanomaterials and the low surface energy properties of the fluorosurfactants, a hydrophobic surface can be constructed with a contact angle over 120° on the strongly hydrophilic quartz surface.[19–21]

In oil/gas reservoirs, after the core pore structure is modified by the composite system, the hydrophobicity of the pore surface is greatly increased, resulting in a sharp decrease in capillary

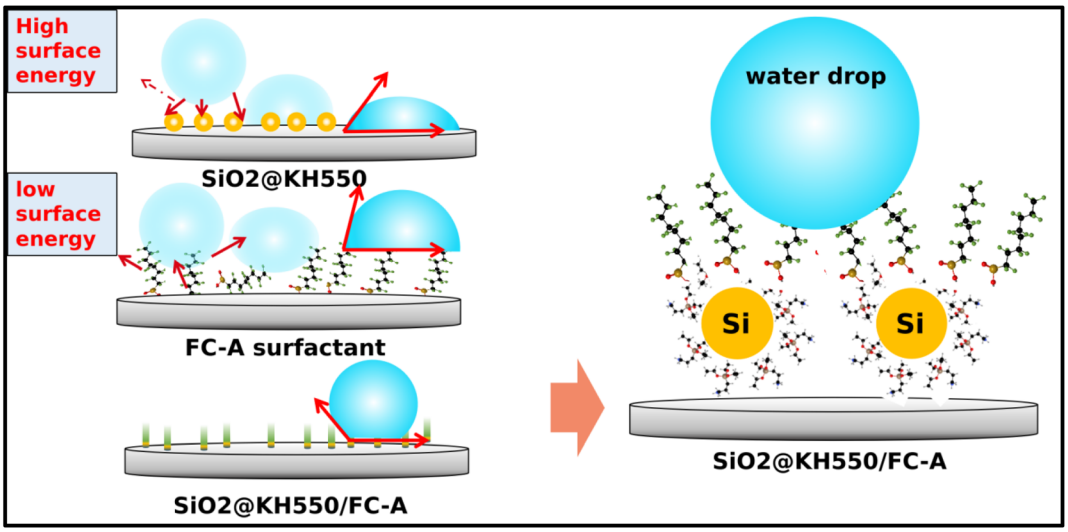

Fig. 15 Schematic illustration of the wettability modification by various fluids.

 © 2025 The Author(s). Published by the Royal Society of Chemistry

Open Access Article. Published on 17 February 2025. Downloaded on 1/22/2026 7:04:25 AM.
This article is licensed under a Creative Commons Attribution-NonCommercial 3.0 Unported Licence.

force, and even the capillary driving force can be transformed into a repulsive force. This would result in difficulty for external fluids to spontaneously absorb into formation pores through formation capillary mechanics, thus greatly reducing fluid imbibition, increasing flowback efficiency, and effectively reducing aqueous phase trap damage in tight sandstone.[27]

5 Conclusions

We prepared a SiO_2@KH550/FC-A nanocomposite system to construct hydrophobic surfaces in cores. First, surface modification of nano-SiO_2 with KH550 was carried out to prepare nanoparticles with good dispersion. FTIR, XRD, SEM, and TG were used to characterize the nanoparticles before and after modification, which verified the success of modification. The fluorinated surfactant FC-A was prepared in the laboratory and compounded with SiO_2@KH550. The system increased the contact angle of the hydrophilic surface from approximately 20° to 130°, so as to achieve wetting modification. The stability is strong, and the contact angle did not significantly decrease within 5 minutes. The SEM and EDS results showed that after treatment with the composite system, a layer of micro and nanoscale particles was attached to the hydrophilic surface, and the surface content of F, Si and O elements was high. It was proved that SiO_2@KH550 and FC-A were adsorbed on the surface, forming a solid interface with a low surface free energy at the micro and nanoscale, which greatly reduced the hydrophilicity.

The results of core self-imbibition experiments confirmed that the construction of a hydrophobic surface can significantly reduce the self-imbibition of core pores to external fluids. In the SiO_2@KH550/FC-A system, the imbibition amount of the core was very small, at only 0.5 mL after 8 hours. Additionally, the maximum imbibition rate was only 0.04 g min^{-1}, and also rapidly decreased to 0.0004 g min^{-1} within 5 minutes. The water saturation of the core treated with the SiO_2@KH550/FC-A composite system decreased to 16.3%, respectively, and the permeability recovered to 88.4%, indicating that the SiO_2@KH550/FC-A composite system can significantly improve the liquid phase flowback ability.

Data availability

All the data from the study are contained in this paper.

Author contributions

Conceptualization: Seqiang Zhuo and Nanxin Yin; data curation: Qun Cheng; formal analysis: Seqiang Zhuo, Chao Luo, and Xinyue Wang; funding acquisition: Songze Li; investigation: Min Jia and Qun Cheng; methodology: Cen Chen and Hong Ren; project administration: Songze Li; resources: Min Jia; software: Nanxin Yin and Chao Luo; validation: Nanxin Yin and Hong Ren; writing – original draft: Cen Chen; writing – review and editing: Xinyue Wang.

Conflicts of interest

There are no conflicts to declare.

Acknowledgements

This article was supported by the Science and Technology Research Program of the Chongqing Municipal Education Commission, Research on fractal characterization of complex fracture networks in mid to deep continental shale gas reservoirs based on the combination of physical modulus and geological modeling (Grant No. KJQN202201505). Also supported by the General Program of Chongqing Natural Science Foundation, Research on the coupling mechanism and classification characterization of natural artificial fractures in terrestrial shale gas reservoirs (Grant No. CSTB2023NSCQ-MSX0044).

Notes and references

1 J. O. Alvarez and D. S. Schechter, Wettability Alteration and Spontaneous Imbibition in Unconventional Liquid Reservoirs by Surfactant Additives, *SPE Reserv. Eval. Eng.*, 2017, **20**, 107–117, DOI: 10.2118/177057-PA.
2 J. Cai, E. Perfect, C.-L. Cheng and X. Hu, Generalized Modeling of Spontaneous Imbibition Based on Hagen–Poiseuille Flow in Tortuous Capillaries with Variably Shaped Apertures, *Langmuir*, 2014, **30**, 5142–5151, DOI: 10.1021/la5007204.
3 A. Dehghan Monfared, M. H. Ghazanfari, M. Jamialahmadi and A. Helalizadeh, Adsorption of silica nanoparticles onto calcite: equilibrium, kinetic, thermodynamic and DLVO analysis, *Chem. Eng. J.*, 2015, **281**, 334–344, DOI: 10.1016/j.cej.2015.06.104.
4 K. Jarrahian, O. Seiedi, M. Sheykhan, M. V. Sefti and S. Ayatollahi, Wettability alteration of carbonate rocks by surfactants: a mechanistic study, *Colloids Surf., A*, 2012, **410**, 1–10, DOI: 10.1016/j.colsurfa.2012.06.007.
5 J. Jin, Y. Wang, T. A. Nguyen, A. V. Nguyen, M. Wei and B. Bai, The effect of gas-wetting nano-particle on the fluid flowing behavior in porous media, *Fuel*, 2017, 431–441.
6 X. Liu, Y. Kang, P. Luo, L. You, Y. Tang and L. Kong, Wettability modification by fluoride and its application in aqueous phase trapping damage removal in tight sandstone reservoirs, *J. Pet. Sci. Eng.*, 2015, **133**, 201–207, DOI: 10.1016/j.petrol.2015.06.013.
7 Q. Meng, H. Liu and J. Wang, A critical review on fundamental mechanisms of spontaneous imbibition and the impact of boundary condition, fluid viscosity and wettability, *Adv. Geo-Energy Res.*, 2017, **1**, 1–17.
8 G. Ni, W. Cheng, B. Lin and C. Zhai, Experimental study on removing water blocking effect (WBE) from two aspects of the pore negative pressure and surfactants, *J. Nat. Gas Sci. Eng.*, 2016, **31**, 596–602, DOI: 10.1016/j.jngse.2016.03.066.
9 M. Salehi, S. J. Johnson and J.-T. Liang, Mechanistic Study of Wettability Alteration Using Surfactants with Applications in

Open Access Article. Published on 17 February 2025. Downloaded on 1/22/2026 7:04:25 AM.
This article is licensed under a Creative Commons Attribution-NonCommercial 3.0 Unported Licence.

Naturally Fractured Reservoirs, *Langmuir*, 2008, **24**, 14099–14107, DOI: 10.1021/la802464u.

10 Y. Xia, Z. Yang, R. Zhang, Y. Xing and X. Gui, Enhancement of the surface hydrophobicity of low-rank coal by adsorbing DTAB: an experimental and molecular dynamics simulation study, *Fuel*, 2019, **239**, 145–152, DOI: 10.1016/j.fuel.2018.10.156.

11 M. M. Fahes and A. Firoozabadi, Wettability alteration to intermediate gas-wetting in gas-condensate reservoirs at high temperatures, *SPE J.*, 2007, **12**, 397–407.

12 M. Aminnaji, H. Fazeli, A. Bahramian, S. Gerami and H. Ghojavand, Wettability alteration of reservoir rocks from liquid wetting to gas wetting using nanofluid, *Transp. Porous Media*, 2015, **109**, 201–216.

13 Z. Xiong, J. Huang, Y. Wu and X. Gong, Robust multifunctional fluorine-free superhydrophobic fabrics for high-efficiency oil–water separation with ultrahigh flux, *Nanoscale*, 2022, **14**, 5840–5850.

14 Z. S. Saifaldeen, K. R. Khedir, M. T. Camci, A. Ucar, S. Suzer and T. Karabacak, The effect of polar end of long-chain fluorocarbon oligomers in promoting the superamphiphobic property over multi-scale rough Al alloy surfaces, *Appl. Surf. Sci.*, 2016, **379**, 55–65.

15 Y. Zhao, C. Yu, H. Lan, M. Cao and L. Jiang, Improved Interfacial Floatability of Superhydrophobic/Superhydrophilic Janus Sheet Inspired by Lotus Leaf, *Adv. Funct. Mater.*, 2017, **27**, 1701466.

16 X. Yang, K. Yu, F. Ji, T. Nie, K. Li and T. Bai, Mechanical Properties of SiO_2/KH560 Modified Basalt Fiber Reinforced Concrete, *Bull. Chin. Ceram. Soc.*, 2024, **43**, 102–112.

17 G. Ni, W. Cheng, B. Lin and C. Zhai, Experimental study on removing water blocking effect (WBE) from two aspects of the pore negative pressure and surfactants, *J. Nat. Gas Sci. Eng.*, 2016, **31**, 596–602.

18 G. Para, E. Jarek and P. Warszynski, The Hofmeister series effect in adsorption of cationic surfactants—theoretical description and experimental results, *Adv. Colloid Interface Sci.*, 2006, **122**, 39–55.

19 M. A. Mousavi, S. Hassanajili and M. R. Rahimpour, Synthesis of fluorinated nano-silica and its application in wettability alteration near-wellbore region in gas condensate reservoirs, *Appl. Surf. Sci.*, 2013, **273**, 205–214.

20 R. Saboori, R. Azin, S. Osfouri, S. Sabbaghi and A. Bahramian, Wettability alteration of carbonate rocks from strongly liquid-wetting to strongly gas-wetting by fluorine-doped silica coated by fluorosilane, *J. Dispersion Sci. Technol.*, 2018, **39**(6), 767–776.

21 L. Wang, K. Yin, Q. Deng, Q. Huang and C. J. Arnusch, Multiscale hybrid-structured femtosecond laser-induced graphene with outstanding photo-electro-thermal effects for all-day anti-icing/deicing, *Carbon*, 2024, **219**, 118824.

22 P. Yang, K. Yin, X. Song, L. Wang, Q. Deng, J. Pei and C. J. Arnusch, Airflow triggered water film self-sculpturing on femtosecond laser-induced heterogeneously wetted micro/nanostructured surfaces, *Nano Lett.*, 2024, **24**(10), 3133–3141.

23 Y. He, K. Yin, L. Wang, T. Wu, Y. Chen and C. J. Arnusch, Femtosecond laser structured black superhydrophobic cork for efficient solar-driven cleanup of crude oil, *Appl. Phys. Lett.*, 2024, **124**, 171601.

24 T. Wu, K. Yin, J. Pei, Y. He, J. A. Duan and C. J. Arnusch, Femtosecond laser-textured superhydrophilic coral-like structures spread AgNWs enable strong thermal camouflage and anti-counterfeiting, *Appl. Phys. Lett.*, 2024, **124**, 161602.

25 Y. Sun, Z. Zhang and C. P. Wong, Study on mono-dispersed nano-size silica by surface modification for underfill applications, *J. Colloid Interface Sci.*, 2005, **292**, 436–444.

26 Y. F. Liu, L. Zhou, X. C. Wan, Y. F. Tang, Q. Liu, W. Li and J. B. Liao, Synthesis and characterization of a temperature sensitive microcapsule gelling agent for high-temperature acid release, *ACS Omega*, 2024, **9**, 20849–20858.

27 Y. Cai, J. Li, L. Yi, X. Yan and J. Li, Fabricating superhydrophobic and oleophobic surface with silica nanoparticles modified by silanes and environment-friendly fluorinated chemicals, *Appl. Surf. Sci.*, 2018, **450**, 102–111.

 © 2025 The Author(s). Published by the Royal Society of Chemistry